Received: 18 November 2016 | Revised: 1 June 2017 | Accepted: 20 July 2017

DOI: 10.1002/stc.2084

RESEARCH ARTICLE

WILEY

Adaptive constrained unscented Kalman filtering for real-time nonlinear structural system identification

Andrea Calabrese[1] | Salvatore Strano[2] | Mario Terzo[2]

[1] Civil Engineering and Construction Engineering Management (CECEM), California State University, Long Beach, CA, USA

[2] Department of Industrial Engineering, University of Naples Federico II, Naples 80125, Italy

Correspondence
Salvatore Strano, Department of Industrial Engineering, University of Naples Federico II, Naples 80125, Italy.
Email: salvatore.strano@unina.it

Summary

The unscented Kalman filter (UKF) is often used for nonlinear system identification in civil engineering; nevertheless, the application of the UKF to highly nonlinear structures could not provide accurate results. In this paper, an improvement of the UKF algorithm has been adopted. This methodology can consider state constraints, and it can estimate the measurement noise covariance matrix. The results obtained adopting a modified UKF have been compared to the ones obtained using the UKF for parameter estimation of a single degree of freedom nonlinear hysteretic system. The second part of this work shows results of an experimental activity on a base-isolated prototype structure. Both numerical and experimental results underline that the adopted algorithm produces better state estimation and parameter identification than the UKF, being capable of taking into account parameter boundaries. The adopted algorithm is more robust than the standard UKF in the case of measuring noise variation.

KEYWORDS

adaptive Kalman filter—nonlinear system identification, constrained unscented Kalman filter, hysteresis, structural dynamics

1 | INTRODUCTION

The identification of nonlinear structural systems is a common task in civil engineering. For example, several methods for damage detection and monitoring of civil engineering structures are based on parametric identification algorithms suitable for nonlinear structural elements.[1–3] Various techniques have been developed for nonlinear structural system identification, including least squares estimation, Monte Carlo filter, extended Kalman filter (EKF), unscented Kalman filter (UKF), and others.[4–11] The time-domain methods, such as the least squares estimation, perform an optimization for parameters such as stiffness and damping through a minimization of the errors between the measured and the simulated responses,[12] but the procedure is time consuming and it is generally considered not suitable for real-time applications of structural health monitoring and damage detection. Monte Carlo filter often requires a very large number of sample points, being high computationally demanding. Among the different methods, the UKF is the most adopted technique for structural dynamics identification with many successful applications.[13–18]

Despite the fact that the UKF outperforms the other methods, especially in presence of very noisy measurements, some deficiencies still remain. One of the most important deficiencies of UKF is the impossibility of taking into account bounds and other constraints on state variables. The constraints can be useful as a remediation for inaccurate system modeling, which often happens in real-world applications. As a consequence, many approaches have been developed

for UKF with constrained problems or called constrained UKF (CUKF).[19–25] In many applications, process and measurement noise covariance matrices are considered known and constant for UKF or CUKF. A wrong selection of these matrices may cause a large estimation error. In some cases, the procedure might not converge.[26] Generally, the task of finding suitable process and measurement noise covariance matrices when using the classical method is time consuming. In addition, measurement noise covariance can vary in actual applications due to electromagnetic interference between sensors and other electrical instruments. To address this problem, an adaptive approach for the CUKF (ACUKF) with an adaptive identification of the measurement noise covariance matrix has been adopted in the present research activity. The major function of adaptive algorithm is to get the measurement noise covariance matrix based on the filter learning history.[26]

In this paper, the ACUKF and the UKF have been applied to a highly nonlinear hysteresis system based on the normalized Bouc-Wen model (NBWM) for the numerical evaluation of both methods.

Nonlinearity of the Bouc-Wen model introduces a complexity for parameter identification. Several methods, based on different approaches, have been proposed.[27,28] In previous studies,[29,30] an identification method for the NBWM has been developed starting from the analytical description of the hysteresis loop developed in Ikhouane and Rodellar.[31] An attractive way to identify the Bouc-Wen model parameters, taking into account measurement noise and model uncertainties, is based on nonlinear filtering, using for example the EKF or the UKF. Yang and Ma[32] proposed an EKF with a global weighted iteration strategy, which was effective in estimating all the parameters of the Bouc-Wen model of hysteresis. Zhang et al.[33] also applied the EKF for the identification of hysteretic systems that exhibit degradation and pinching.

In literature,[34–38] the UKF has been used for the identification of nondegrading and degrading hysteretic systems.

The ACUKF and the UKF have been applied to an actual base-isolated structure prototype. The experimental results have been adopted for a further comparison between the estimation methods.

The paper is organized as follows: A description of the UKF and the ACUKF is given in Section 2. Simulation results are presented in Section 3. The experimental testing of both methods on the prototype structure is detailed in Section 4.

2 | THE ALGORITHMS OF UKF AND ACUKF

2.1 | UKF

The UKF has been first proposed by Julier and Uhlman[39] and further improved.[40] Because UKF does not require valuating Jacobian and Hessian matrices and has superior accuracy compared to EKF in terms of approximating the statistics of highly nonlinear systems, it is suitable for estimating fairly complex dynamical systems. In the unscented transformation, the statistical properties of a random variable are approximated by a deterministically chosen sample of points known as sigma points. The nonlinear transformation is applied to each of the sigma points, and the statistical properties of the transformed random variable are calculated from the transformed sample set.

The UKF algorithm is briefly recalled in the following because it has been adopted for a comparative analysis. Consider the following continuous nonlinear state space description with discrete measurements sampled at regular intervals with sampling period Δt

$$\begin{aligned} \mathbf{x}_{k+1} &= \mathbf{x}_k + \int_{k\Delta t}^{(k+1)\Delta t} \mathbf{f}[\mathbf{x}(\tau), \mathbf{u}(\tau)]d\tau + \mathbf{w}_k \quad \mathbf{x}_k \equiv \mathbf{x}(k\Delta t) \\ \mathbf{y}_{k+1} &= \mathbf{h}(\mathbf{x}_{k+1}, \mathbf{u}_{k+1}) + \mathbf{v}_{k+1} \end{aligned} \tag{1}$$

where $\mathbf{x} \in \mathbf{R}^n$ is the n-dimensional vector of system state, $\mathbf{f}$ and $\mathbf{h}$ are nonlinear functions, $\mathbf{u}$ is the input vector, $\mathbf{w}$ is the process noise with covariance $\mathbf{Q}$, $\mathbf{y} \in \mathbf{R}^m$ is the m-dimensional vector of measurement, $\mathbf{v}$ is the Gaussian white measurement noise with covariance $\mathbf{R}$, and k is the kth time step. The main task is to estimate the system state, that is, calculate the mean as well as the covariance of system state at the $(k + 1)$th step, based on the state estimation at the kth step and the measurements at the current $(k + 1)$th step.

Given the filtered state estimates $\widehat{\mathbf{x}}_{k \mid k}$, which have been obtained using all the measurements made up to time t_k, and the input $\mathbf{u}_k$, the predicted state estimates $\widehat{\mathbf{x}}_{k+1 \mid k}$ can be obtained as

$$\widehat{\mathbf{x}}_{k+1\mid k}=\widehat{\mathbf{x}}_{k\mid k}+\int_{k\Delta t}^{(k+1)\Delta t}\mathbf{f}[\mathbf{x}(\tau),\mathbf{u}_k]d\tau;\quad \widehat{\mathbf{x}}_{k\mid k}\equiv\widehat{\mathbf{x}}(k\Delta t). \tag{2}$$

A set of $2n+1$ sigma points $\mathbf{X}_{k\mid k,i}$ with associated weights $\mathbf{W}_i$ are chosen symmetrically about $\widehat{\mathbf{x}}_{k\mid k}$ as follows:

$$\begin{aligned}&\mathbf{X}_{k\mid k,0}=\widehat{\mathbf{x}}_{k\mid k},\quad \mathbf{W}_0=\frac{\kappa}{n+\kappa},\\&\mathbf{X}_{k\mid k,i}=\widehat{\mathbf{x}}_{k\mid k}+\left(\sqrt{(n+\kappa)\mathbf{P}_{k\mid k}}\right)_i,\quad \mathbf{W}_{\mathrm{i}}=\frac{1}{2(n+\kappa)},\\&\text{and}\\&\mathbf{X}_{k\mid k,i+n}=\widehat{\mathbf{x}}_{k\mid k}-\left(\sqrt{(n+\kappa)\mathbf{P}_{k\mid k}}\right)_i,\quad \mathbf{W}_{\mathrm{i+n}}=\frac{1}{2(n+\kappa)},\end{aligned} \tag{3}$$

where $\left(\sqrt{\mathbf{P}_{k\mid k}}\right)_i$ is the ith column of the matrix square root of the error covariance matrix $\mathbf{P}_{k\mid k}$ and $\mathbf{W}_i$ is the weights associated with the corresponding point. The parameter κ is a tuning parameter and it has been recommended that its value be chosen such $\kappa+n=3$. However, if the dimension of the system is greater than three, κ can take a negative value and, in such a case, the covariance matrices may become indefinite. In all our simulations, it has been chosen $\kappa=1$.

Because the weights $\mathbf{W}_i$ sum to 1 and due to the symmetric placement of the sigma points, the weighted mean of the set $\mathbf{X}$ is the same as $\widehat{\mathbf{x}}_{k\mid k}$. This choice also ensures that the weighted covariance matrix of the sample $\mathbf{X}$ is equal to $\mathbf{P}_{k\mid k}$, that is,

$$\mathbf{P}_{k\mid k}=\sum_{i=0}^{2n}\mathbf{W}_{k,i}\left(\mathbf{X}_{k\mid k,i}-\widehat{\mathbf{x}}_{k\mid k}\right)\left(\mathbf{X}_{k\mid k,i}-\widehat{\mathbf{x}}_{k\mid k}\right)^{\mathrm{T}}, \tag{4}$$

In the prediction step, the sigma points are propagated through the nonlinear state space equation to obtain the predicted set of sigma points as

$$\mathbf{X}_{k+1\mid k,i}=\widehat{\mathbf{x}}_{k\mid k,i}+\int_{k\Delta t}^{(k+1)\Delta t}\mathbf{f}[\mathbf{X}_i(\tau),\mathbf{u}_k]d\tau;\quad \mathbf{X}_{k\mid k,i}\equiv\mathbf{X}_i(k\Delta t)\ . \tag{5}$$

The predicted state estimate and its error covariance matrix are obtained from the predicted sigma points as

$$\begin{aligned}\widehat{\mathbf{x}}_{k+1\mid k}&=\sum_{i=0}^{2n}\mathbf{W}_{k,i}\mathbf{X}_{k+1\mid k,i}\\\mathbf{P}_{k+1\mid k}&=\sum_{i=0}^{2n}\mathbf{W}_{k,i}\left(\mathbf{X}_{k+1\mid k,i}-\widehat{\mathbf{x}}_{k+1\mid k}\right)\left(\mathbf{X}_{k+1\mid k,i}-\widehat{\mathbf{x}}_{k+1\mid k}\right)^{\mathrm{T}}+\mathbf{Q}_k.\end{aligned} \tag{6}$$

For obtaining the updated state estimate, the sigma points are propagated through the nonlinear measurement equation to obtain the predicted measurements as

$$\mathbf{Y}_{k+1\mid k,i}=\mathbf{h}\left(\mathbf{X}_{k+1\mid k,i},\mathbf{u}_{k+1}\right),\quad i=0,1,...,2n. \tag{7}$$

Using this set of predicted measurements, the covariance matrix of innovations (difference between measurement and predicted measurement) and the cross-covariance matrix between predicted state estimate errors and innovations are computed as

$$\begin{aligned}\mathbf{P}_{yy,k+1\mid k}&=\sum_{i=0}^{2n}\mathbf{W}_{k,i}\left(\mathbf{Y}_{k+1\mid k,i}-\widehat{\mathbf{y}}_{k+1\mid k}\right)\left(\mathbf{Y}_{k+1\mid k,i}-\widehat{\mathbf{y}}_{k+1\mid k}\right)^{\mathrm{T}}+\mathbf{R}_{k+1}\\\mathbf{P}_{xy,k+1\mid k}&=\sum_{i=0}^{2n}\mathbf{W}_{k,i}\left(\mathbf{X}_{k+1\mid k,i}-\widehat{\mathbf{x}}_{k+1\mid k}\right)\left(\mathbf{Y}_{k+1\mid k,i}-\widehat{\mathbf{y}}_{k+1\mid k}\right)^{\mathrm{T}},\end{aligned} \tag{8}$$

where

$$\widehat{\mathbf{y}}_{k+1\mid k} = \sum_{i=0}^{2n} \mathbf{W}_{k,i}\mathbf{Y}_{k+1\mid k,i}. \tag{9}$$

The preceding two covariance matrices are used to compute the Kalman gain matrix

$$\mathbf{K}_{k+1} = \mathbf{P}_{xy,k+1\mid k}\left(\mathbf{P}_{yy,k+1\mid k}\right)^{-1}, \tag{10}$$

and finally, the updated state estimates are obtained using the linear update equation as in the Kalman filter

$$\widehat{\mathbf{x}}_{k+1\mid k+1} = \widehat{\mathbf{x}}_{k+1\mid k} + \mathbf{K}_{k+1}\left(\mathbf{y}_{k+1} - \widehat{\mathbf{y}}_{k+1\mid k}\right). \tag{11}$$

The covariance matrix of error in the updated state estimates is computed using

$$\mathbf{P}_{k+1\mid k+1} = \mathbf{P}_{k+1\mid k} - \mathbf{K}_{k+1}\,\mathbf{P}_{yy,k+1\mid k}\mathbf{K}_{k+1}^{\mathrm{T}}. \tag{12}$$

2.2 | ACUKF

An improved version of the UKF is the CUKF, introduced in Section 1, which can take into account constraints of the state variables.

The CUKF approach considered in this paper consists of two main aspects[25]: (a) In prediction step, sigma points that violate bound constraints are moved onto the bounds, and the relevant sigma points within the boundary are moved correspondingly in order to obtain the symmetry of the new set of sigma points; (b) in correction step, the state updating equation is used to generate transformed sigma points, and those transformed sigma points that violate bound constraints are projected to constraints boundary only when the updated state estimate exceeds the boundary.[25] The details of above proposals are described as follows.

Consider the nonlinear dynamic system given by (1). In addition, bound constraints are imposed to the states as

$$\mathbf{x}_L \le \mathbf{x} \le \mathbf{x}_U, \tag{13}$$

where $\boldsymbol{x}_U$ and $\boldsymbol{x}_L$ are the upper and lower bound of constrained vectors, respectively.

Indicating with $\widehat{\mathbf{x}}_{k\mid k}$ the filtered state estimates at time instant "k" and $\mathbf{P}_{k\mid k}$ the corresponding estimate error covariance matrix and denoting with

$$\begin{aligned}\mathbf{s}_{i,k} &= \left(\sqrt{\mathbf{P}_{k\mid k}}\right)_i \\ \mathbf{s}_{n+1,k} &= -\left(\sqrt{\mathbf{P}_{k\mid k}}\right)_i,\end{aligned} \tag{14}$$

as the directions along which the sigma points are selected, according to the standard UKF, the step sizes for all sigma points, for the simple case when only bound constraints are considered, can be performed as follows[24]:

$$\begin{aligned}\theta_{k,i} = \theta_{k,n+i} &= \min\left(\theta_{k,i}^{C}, \theta_{k,n+i}^{C}\right), && i = 1,\ldots,n \\ \theta_{k,i}^{C} &= \min\left(\sqrt{n+\kappa}, \theta_{k,i}^{U}, \theta_{k,i}^{L}\right), && i = 1,\ldots,2n \\ \theta_{k,i}^{U} &= \min\left(\infty, \frac{(\mathbf{x}_U)_j - \left(\widehat{\mathbf{x}}_{k\mid k}\right)_j}{\left(\mathbf{s}_{k,i}\right)_j}\right), && \text{if } \left(\mathbf{s}_{k,i}\right)_j > 0, \quad i = 1,\ldots,2n \\ \theta_{k,i}^{L} &= \min\left(\infty, \frac{(\mathbf{x}_L)_j - \left(\widehat{\mathbf{x}}_{k\mid k}\right)_j}{\left(\mathbf{s}_{k,i}\right)_j}\right), && \text{if } \left(\mathbf{s}_{k,i}\right)_j < 0, \quad i = 1,\ldots,2n,\end{aligned} \tag{15}$$

where the subscript j represents the jth element of the vector $\mathbf{x}$.

If the current estimate is sufficiently far from the bounds, or in the absence of bounds, the above choice of sigma points is identical to those used in UKF. If the current estimate is close to the bounds, then the above choice ensures that none of the sigma points violate the bounds on state variables.

The weights of all of sigma points are adjusted by using a linear weighting method proposed in Vachhani et al[21]:

$$\begin{aligned} \mathbf{W}_{k,0} &= b, \quad i = 0 \\ \mathbf{W}_{k,i} &= a\theta_{k,i} + b, \quad i = 1, ..., 2n, \end{aligned} \tag{16}$$

where

$$\begin{aligned} a &= \frac{2\kappa\text{-}1}{2(n+\kappa)\left[s_k - (2n+1)\sqrt{n+\kappa}\right]} \\ b &= \frac{1}{2(n+\kappa)} - \frac{2\kappa\text{-}1}{2\sqrt{n+\kappa}\left[s_k - (2n+1)\sqrt{n+\kappa}\right]}. \\ s_k &= \sum_{i=1}^{2n} \theta_{k,i} \end{aligned} \tag{17}$$

The replacement of sigma points results in a first-order accuracy for the unscented transformation of mean value if $\kappa = 0.5$, that is, the value adopted in this paper.

Each sigma point $\mathbf{X}_{k \mid k,i}$ is transformed through the state-space equation in order to obtain sigma point of state prediction $\mathbf{X}_{k+1 \mid k,i}$, the mean of the predicted state estimate $\widehat{\mathbf{x}}_{k+1 \mid k}$, and its error covariance matrix $\mathbf{P}_{k+1 \mid k}$, as well as the calculation of the predicted measurement sigma points $\mathbf{Y}_{k+1 \mid k,i}$, the mean $\widehat{\mathbf{y}}_{k+1 \mid k}$, and covariance matrix $\mathbf{P}_{yy,k+1 \mid k}$ of predicted measurement and the cross-covariance matrix $\mathbf{P}_{xy,k+1 \mid k}$, according to the standard UKF method.

For unconstrained system states, the UKF method adopts state correction equation of the standard Kalman filter to calculate the mean and covariance of the corrected state. For the constrained state estimate, the transformed sigma points can be calculated with Kalman updating equation as

$$\mathbf{X}_{k+1 \mid k+1,i} = \mathbf{X}_{k+1 \mid k,i} + \mathbf{K}_{k+1}\left(\mathbf{y}_{k+1} - \mathbf{Y}_{k+1 \mid k,i}\right), i = 0, 1, ..., 2n, \tag{18}$$

in accordance with the method proposed in Kolas et al.[23]

With $\mathbf{X}_{k+1 \mid k+1,i}$ calculated by (18), the state update $\widehat{\mathbf{x}}_{k+1 \mid k+1}$ and its covariance $\mathbf{P}_{k+1 \mid k+1}$ can be calculated using the following equations:

$$\begin{aligned} \widehat{\mathbf{x}}_{k+1 \mid k+1} &= \sum_{i=0}^{2n} \mathbf{W}_{k,i} \mathbf{X}_{k+1 \mid k+1,i} \\ \mathbf{P}_{k+1 \mid k+1} &= \sum_{i=0}^{2n} \mathbf{W}_{k,i} \left(\mathbf{X}_{k+1 \mid k+1,i} - \widehat{\mathbf{x}}_{k+1 \mid k+1}\right)\left(\mathbf{X}_{k+1 \mid k+1,i} - \widehat{\mathbf{x}}_{k+1 \mid k+1}\right)^{\mathrm{T}} + \mathbf{Q}_k + \mathbf{K}_{k+1}\, \mathbf{R}_{k+1}\, \mathbf{K}_{k+1}^{\mathrm{T}}. \end{aligned} \tag{19}$$

It can be proven that the above equations give the same results of the standard UKF in terms of updated mean and covariance.[23,25]

2.2.1 | Adaptation algorithm of measurement noise covariance matrix

In this section, details of the ACUKF, briefly provided in the introduction, are presented. The ACUKF algorithm concerning the matrix $\mathbf{R}$ is described as follows[26]:

$$\begin{aligned} d_{k+1} &= (1-b)/\left(1-b^{k+1}\right), \\ \mathbf{R}_{k+1} &= \mathbf{R}_k + d_{k+1}\left(\boldsymbol{\varepsilon}_{k+1}\boldsymbol{\varepsilon}_{k+1}^{\mathrm{T}} - \mathbf{P}_{yy,k+1 \mid k}\right), \\ \boldsymbol{\varepsilon}_{k+1} &= \mathbf{y}_{k+1} - \mathbf{h}\left(\widehat{\mathbf{x}}_{k+1 \mid k+1}, \mathbf{u}_{k+1}\right) \end{aligned} \tag{20}$$

where d_k is a scaling parameter, b denotes a forgetting factor, usually between 0.95 and 0.995, and ε_k refers to the error between the actual measurement and the filter estimation in the kth step. The positive definiteness of the matrix R in (20) is guaranteed in the adaptation algorithm.

Through the adaptive algorithm, the measurement noise covariance matrix can be computed step by step online.[26] Thus, the system estimation cannot be restricted by the initial noise covariance and can adapt the variable system well.

3 | NUMERICAL EXAMPLE—SDOF NONLINEAR HYSTERETIC SYSTEM

Without loss of generality, consider a single degree of freedom (SDOF) nonlinear hysteretic system subject to an earthquake acceleration, where the hysteresis force is mathematically described by the NBWM[31]

$$m\ddot{x}(t) + c\dot{x}(t) + F(t) = -m\ddot{x}_g(t) \tag{21}$$

where m is the mass, $x(t)$ is the displacement, c is the linear viscous coefficient, $F(t)$ is hysteretic component, and $\ddot{x}_g(t)$ is the excitation acceleration; the overdot indicates derivative with respect to time. The restoring force $F(t)$, based on the NBWM, is

$$\begin{aligned} F(t) &= k_f x(t) + k_w w(t) \\ \dot{w}(t) &= \rho\dot{u}(t)\left\{1 + |w(t)|^n \sigma\left[1 - \operatorname{sgn}(\dot{u}(t)w(t)) - \frac{1}{\sigma}\right]\right\}, \end{aligned} \tag{22}$$

where the parameters of the normalized form of the Bouc-Wen model are ρ, σ, n, k_f, and k_w with the following constraints:

$$\rho > 0; \quad \sigma \geq \frac{1}{2}; \quad n \geq 1; \quad k_f > 0; \quad k_w > 0. \tag{23}$$

Moreover, in Ikhouane and Rodellar,[31] it is demonstrated that $w(t)$ is bounded in the range $[-1, 1]$.

An augmented state vector $\mathbf{x}$ is defined as

$$\mathbf{x} = \begin{bmatrix} x_1 \\ x_2 \\ x_3 \\ x_4 \\ x_5 \\ x_6 \\ x_7 \\ x_8 \\ x_9 \end{bmatrix} = \begin{bmatrix} \dot{x} \\ x \\ w \\ c \\ k_f \\ k_w \\ \rho \\ \sigma \\ n \end{bmatrix}. \tag{24}$$

Then the state space equation is formulated based on Equations 21 and 22 as fallows

$$\dot{\mathbf{x}} = \mathbf{f}(\mathbf{x}(t), \mathbf{u}(t)) = \begin{bmatrix} \dot{x}_1 \\ \dot{x}_2 \\ \dot{x}_3 \\ \dot{x}_4 \\ \dot{x}_5 \\ \dot{x}_6 \\ \dot{x}_7 \\ \dot{x}_8 \\ \dot{x}_9 \end{bmatrix} = \begin{bmatrix} \ddot{x} \\ \dot{x} \\ \dot{w} \\ c \\ \dot{k}_f \\ \dot{k}_w \\ \dot{\rho} \\ \dot{\sigma} \\ \dot{n} \end{bmatrix} = \begin{bmatrix} -\ddot{x}_g - \dfrac{x_2 x_5 + x_1 x_4 + x_3 x_6}{m} \\ x_1 \\ x_7 x_1 \left\{ 1 + |x_3|^{x_9} x_8 \left[1 - \operatorname{sgn}(x_1 x_3) - \dfrac{1}{x_8} \right] \right\} \\ 0 \\ 0 \\ 0 \\ 0 \\ 0 \\ 0 \end{bmatrix}. \tag{25}$$

where u is the base excitation.

The derivatives of the NBWM parameters are all zero because they are assumed to be constant. A discrete time form of (25) is given by

$$\mathbf{x}_{k+1} = \begin{bmatrix} x_{1,k} + \Delta t \left(-\ddot{x}_g - \dfrac{x_{2,k} x_{5,k} + x_{1,k} x_{4,k} + x_{3,k} x_{6,k}}{m} \right) \\ x_{2,k} + \Delta t x_{1,k} \\ x_{3,k} + x_{7,k} x_{1,k} \Delta t \left\{ 1 + \left| x_{3,k} \right|^{x_{9,k}} x_{8,k} \left[1 - \operatorname{sgn}\left(x_{1,k} x_{3,k} \right) - \dfrac{1}{x_{8,k}} \right] \right\} \\ x_{4,k} \\ x_{5,k} \\ x_{6,k} \\ x_{7,k} \\ x_{8,k} \\ x_{9,k} \end{bmatrix} + \mathbf{w}_k, \tag{26}$$

where a process noise $\mathbf{w}$ has been added.

If the acceleration response and excitation are measured, the observation equation can be expressed as

$$y = \ddot{x} + \ddot{x}_g + v, \tag{27}$$

where $\ddot{x}$ is the acceleration of the suspended mass and v represents the measurement noise.

The function **h,** see (1) for reference, can be written as follows

$$\mathbf{y}_{k+1} = \mathbf{h}(\mathbf{x}_{k+1}, \mathbf{u}_{k+1}) + \mathbf{v}_{k+1} = \frac{x_{2,k+1} x_{5,k+1} + x_{1,k+1} x_{4,k+1} + x_{3,k+1} x_{6,k+1}}{m} + v_{k+1}. \tag{28}$$

In accordance with (23), the bound constraints of the ACUKF are

$$-1 \le x_3 \le 1, x_4 > 0, x_5 > 0, x_6 > 0, x_7 > 0, x_8 \ge \frac{1}{2}, x_9 \ge 1, \tag{29}$$

and $w(t)$ is bounded in the range $[-1, 1]$ as demonstrated in Ikhouane and Rodellar.[31] Consequently, the application of the ACUKF to the NBWM is particular suitable to constrain both the parameter values and the state variable w, improving accuracy and robustness of the hysteresis estimation.

Without loss of generality, simulations have been performed by assigning to the model previously described the Chi-Chi earthquake acceleration. In particular, the acceleration time history has a duration of 20 s with its maximum scaled value equal to 3 m/s^2. A measurement noise has been added to the mass acceleration, used as measurement for the parameter estimation. In addition, the measurement noise has been modified at $t = 10$ s (0.0001 and 0.0025 m^2/s^2 before and after $t = 10$ s) in order to analyze the behavior of the ACUKF and the UKF with respect to a sudden variation of the measurement noise.

Figures 1–6 show the estimated parameters compared with the exact ones that are

$c = 100$; $k_f = 100000$; $k_w = 5000$; $\rho = 100$; $\sigma = 0.8$; $n = 2$. The initial parameter values for the estimation are $c = 50$; $k_f = 140000$; $k_w = 8000$; $\rho = 70$; $\sigma = 5$; $n = 5$.

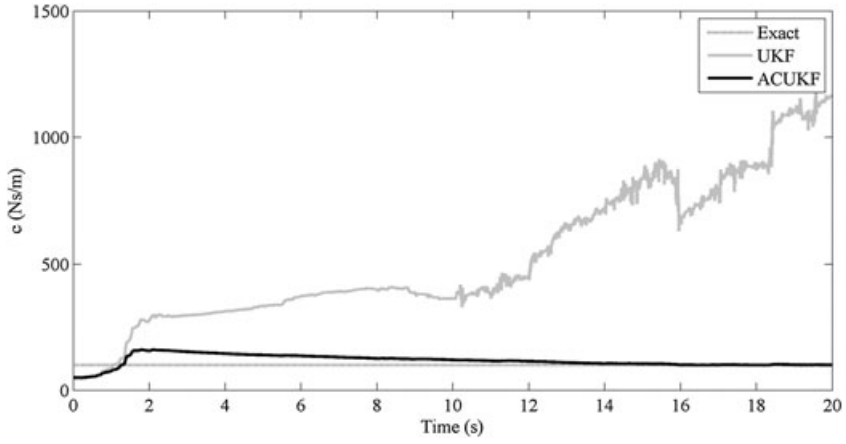

FIGURE 1 Numerical results—Estimation of parameter c

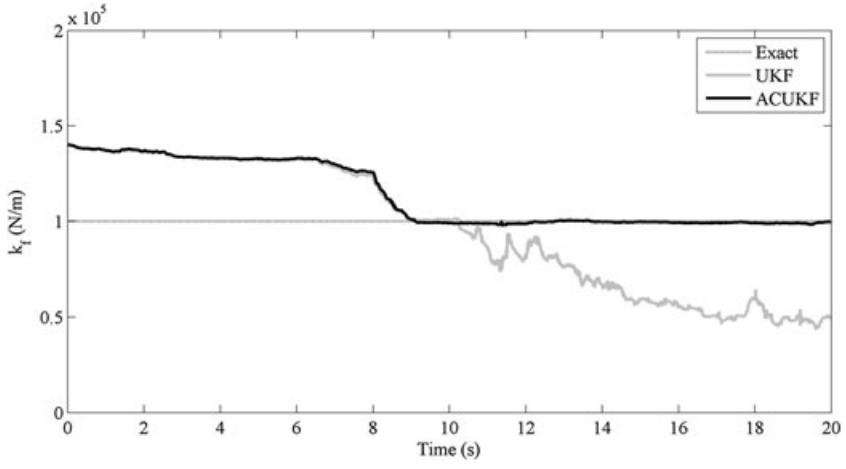

FIGURE 2 Numerical results—Estimation of parameter k_f

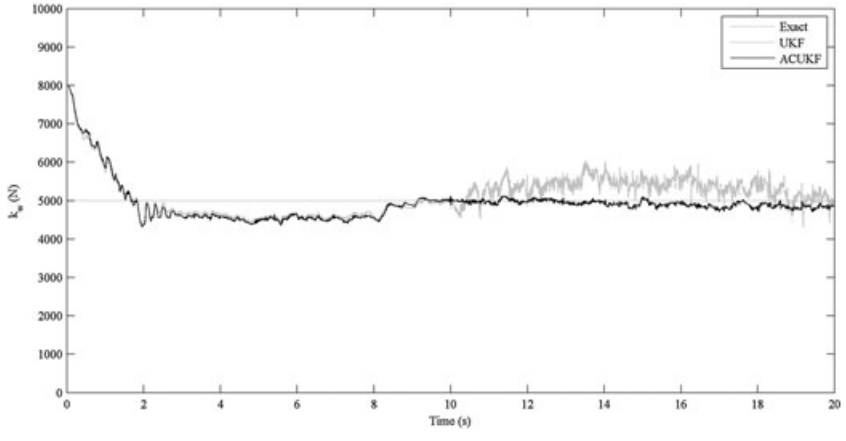

FIGURE 3 Numerical results—Estimation of parameter k_w

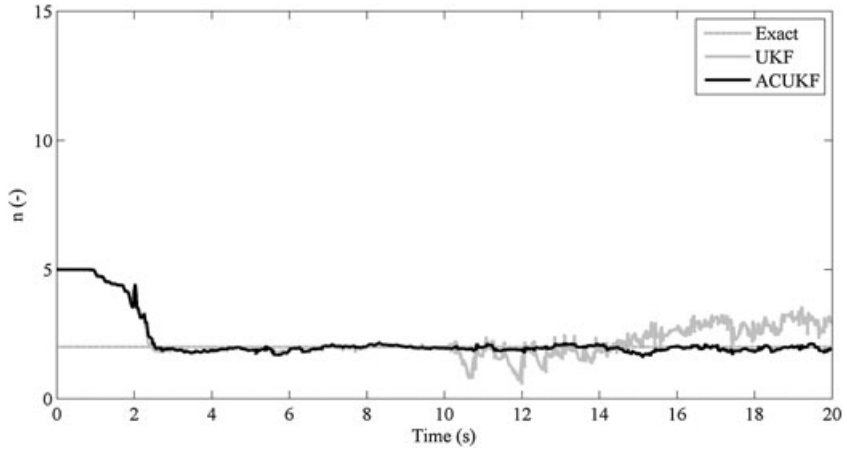

FIGURE 4 Numerical results—Estimation of parameter n

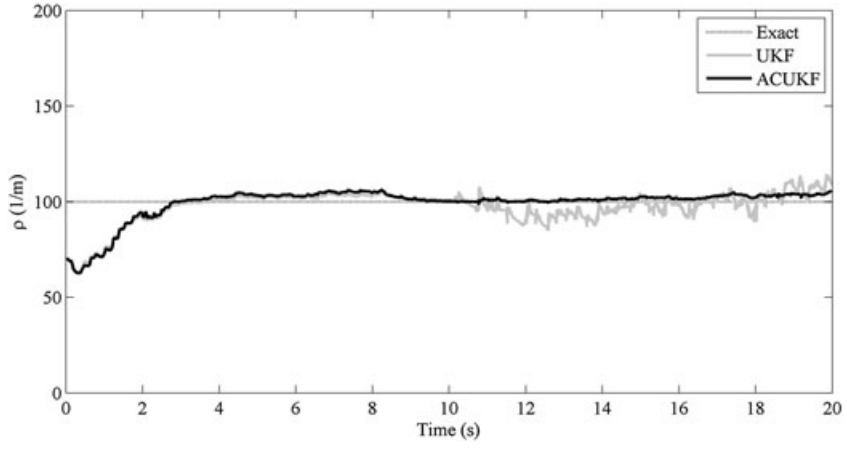

FIGURE 5 Numerical results—Estimation of parameter ρ

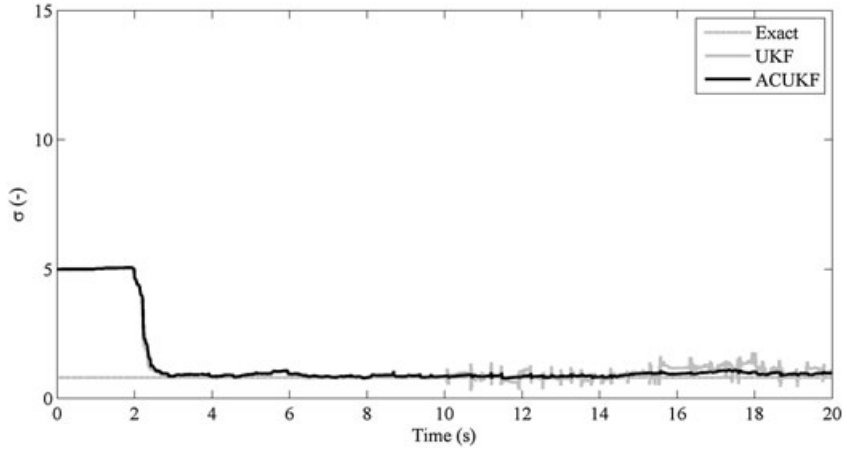

FIGURE 6 Numerical results—Estimation of parameter σ

The results clearly show that the estimator ACUKF demonstrates a better robustness with respect to measurement noise level. Indeed, after a variation of **R**, the parameters estimated with the ACUKF method are very close to exact ones. In contrast, the estimated parameters with the UKF degrades with the variation of **R** as it is possible to note in the figures above. In the first part the noise level is constant, and the value is equal to the one adopted in the UKF; therefore, it is possible to assume that the comparison is between the CUKF (without adaptation) and the UKF. In the second part of the numerical example, the noise level changes and the performance of the adaptation algorithm is verified. Thus, the numerical results show the improvement for parameter estimation of both the state boundaries and the adaptive algorithm. Table 1 shows the root mean square error evaluated in the last 5 s of the simulation and related to the estimated parameters for the UKF and the ACUKF.

TABLE 1 RMSE of the estimated parameters

RMSE/parameters	UKF	ACUKF
c	824.1	2.1
k_f	47722.9	896.9
k_w	376.2	148.3
ρ	5.3	3.1
σ	0.4	0.2
n	0.8	0.1

Note. ACUKF = adaptive constrained unscented Kalman filter; RMSE = root mean square error; UKF = unscented Kalman filter.

For all the parameters, the calculated root mean square errors for the ACUKF are less than those ones relative to the UKF.

Figure 7 presents the estimation of the measurement noise my means of the ACUKF.

The results of Figure 7 show a good matching between the estimated **R** and the exact values before and after the sudden variation of the measurement noise level.

A further comparison between the two methods has been performed considering the displacement estimation of the suspended mass. Figure 8 shows the estimated displacements and the time-history obtained by numerical integration.

Also in this case, the ACUKF performs better than the UKF: The ACUKF provides a displacement estimation that practically matches the exact one.

Simulation results show that the method ACUKF takes into account state constraints and it is robust to variations of **R** due to its adaptive property.

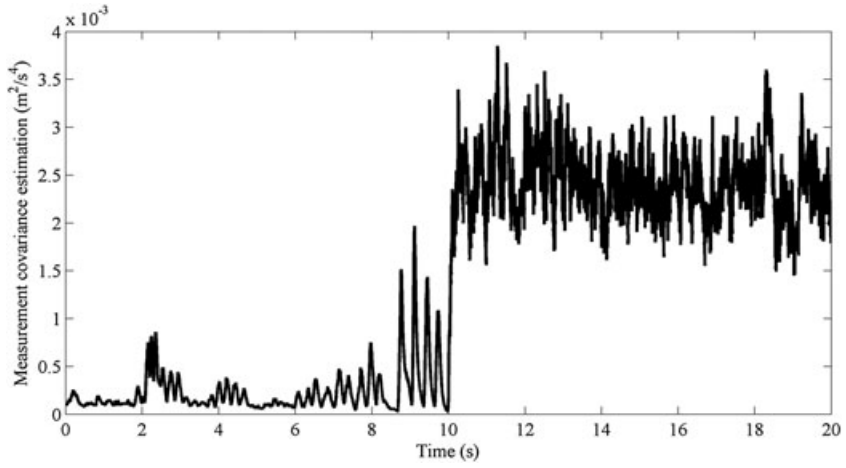

FIGURE 7 Numerical results—Measurement covariance estimation with the ACUKF

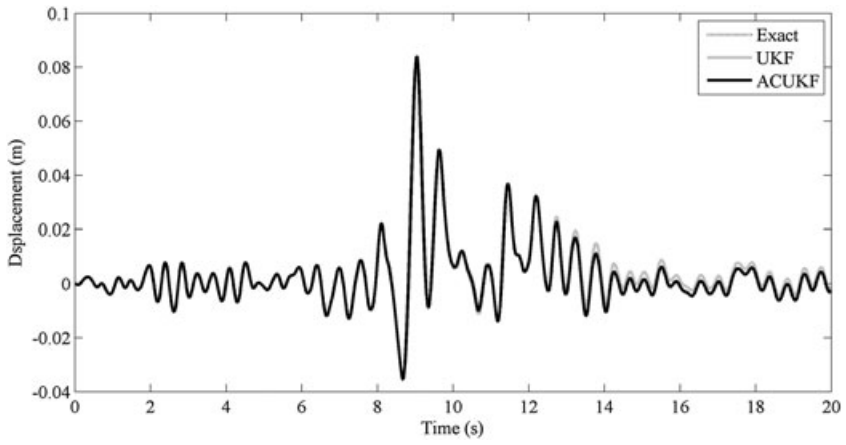

FIGURE 8 Numerical results—Suspended mass displacement estimation

In the next section, some experimental results, concerning the application of the ACUKF and the UKF methods to an actual structure, are presented.

4 | EXPERIMENTAL STUDY

Experimental results, illustrated in this section, have been obtained by imposing to a prototype base-isolated building a seismic event. The tested building is a one-third scale steel frame (Figure 9), base isolated by means of four fiber reinforced bearings.[41–44] It has a total height of 2,900 mm and 2650 × 2150 mm plan dimensions.

The columns of the test building are welded square hollow sections (150 × 150 × 15 mm), whereas the beams are hot formed—square hollow sections (120 × 120 × 12.5 mm). Pin connections are used at the roof level of the building, and a

FIGURE 9 Tested isolated building

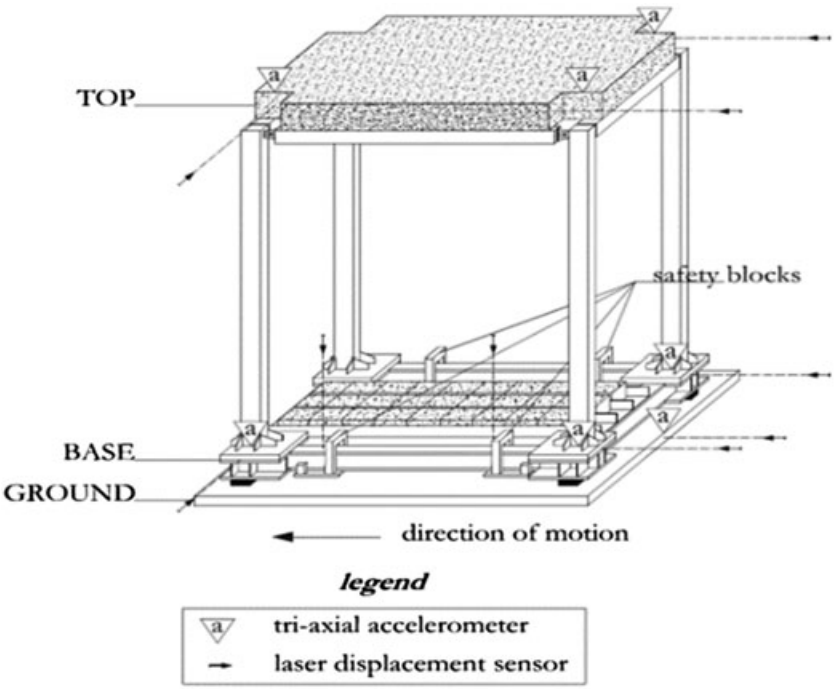

FIGURE 10 Scheme of the prototype building and the instrumentation setup

rigid node is built at the base level of the structure. Each floor has additional concrete blocks to provide a total mass of 7.7 tons. The base level has a mass of 3.6 tons, and the top floor has a mass of 4.1 tons.

Figure 10 shows a projection of the prototype isolated structure and the measuring instruments.

To measure the structural response, nine laser displacement sensors with a resolution of 50 μm have been adopted. Two transducers have been used to measure the absolute displacements of the masses in the direction of the applied motion. The absolute accelerations of the floor masses have been measured by six triaxial accelerometers. The sampling frequency of the measured quantities has been set at 500 Hz, and the signals have been filtered at 50 Hz with a low-pass filter.

The shaking table has been controlled giving as target the acceleration along the direction of motion (Figure 10). Figure 11 shows the seismic event (Campano Lucano, scaled factor SF = 2.06, PGA = 2.55 m/s^2).

The structure dynamics represented by a two degrees of freedom lumped-mass model is given by the following system of ordinary differential equations:

$$\begin{aligned}
&\mathbf{M}\ddot{X} + \mathbf{C}\dot{X} + \mathbf{K}X = -\mathbf{M}\{\mathbf{1}\}\ddot{x}_g - \mathbf{L}F_h \\
&X = \begin{bmatrix} v_b \\ v_t \end{bmatrix} \\
&\mathbf{M} = \begin{bmatrix} m_b & 0 \\ 0 & m_t \end{bmatrix};\ \mathbf{C} = \begin{bmatrix} c_s & -c_s \\ -c_s & c_s \end{bmatrix} \\
&\mathbf{K} = \begin{bmatrix} k_s & -k_s \\ -k_s & k_s \end{bmatrix};\ \mathbf{L} = \begin{bmatrix} n_i \\ 0 \end{bmatrix},
\end{aligned} \tag{30}$$

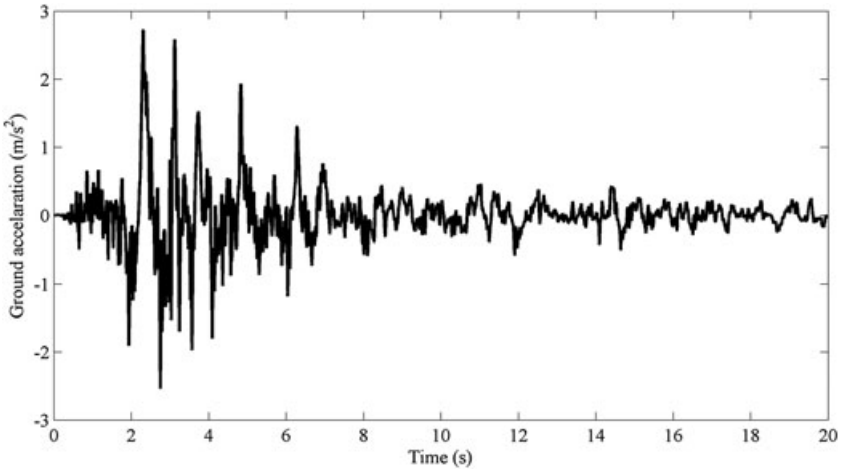

FIGURE 11 Input acceleration to the shaking table

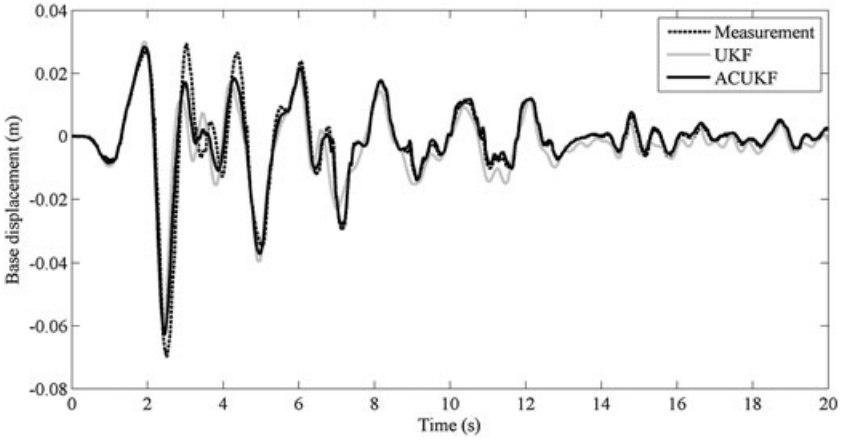

FIGURE 12 Experimental results—Base displacement estimation

where **M**, **K**, and **C** represent the structural mass, stiffness, and damping matrices, respectively; {**1**} is the unit vector, $\ddot{x}_g$ indicates the ground excitation, v_b is the relative displacement of the base to the ground, v_t is the relative displacement of the top to the ground, m_b, m_t, k_s, and c_s are the mass of the base, the mass of the top, the structure linear stiffness, and the structure linear damping, respectively. X, $\dot{X}$, and $\ddot{X}$ represent the structure response in terms of displacement, velocity, and acceleration, respectively. On the right-hand side of Equation 30, F_h is the reaction force (modeled with Equation 22) of each isolator at the base of the structure, n_i is the number of isolators (equal to four), and $\mathbf{M}\{\mathbf{1}\}\ddot{x}_g$ is the effective seismic force. Shaking table tests on the reference structure in its fixed base configuration provided the following values adopted in the estimation algorithms[41]: m_b = 3,571 kg, m_t = 4,155 kg, $k_s = 1{,}845{\cdot}10^6$ N/m, and c_s = 1,751 Ns/m. The mathematical descriptions of the UKF and the ACUKF have been derived from the differential Equations 30.

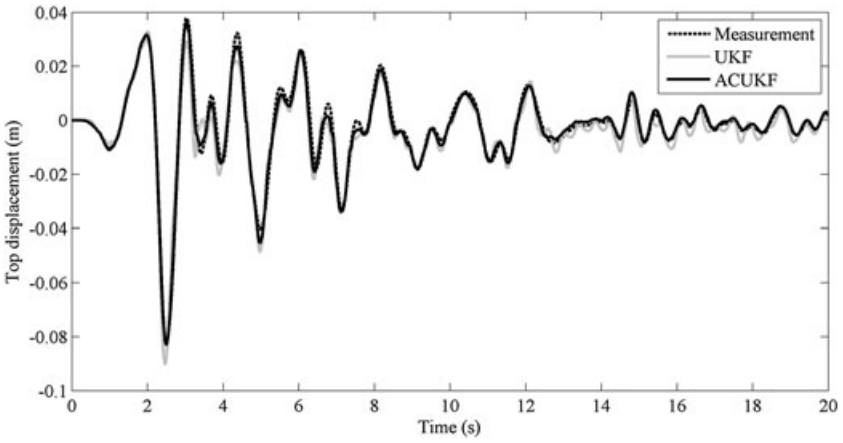

FIGURE 13 Experimental results—top displacement estimation

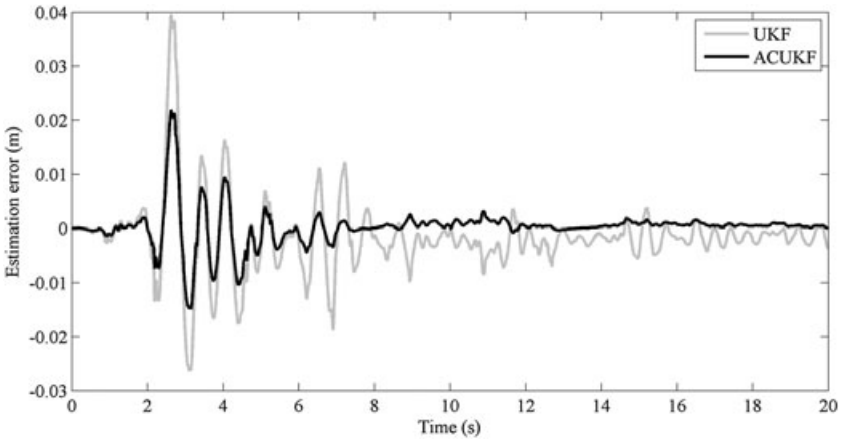

FIGURE 14 Experimental results—Estimation error for the base displacement

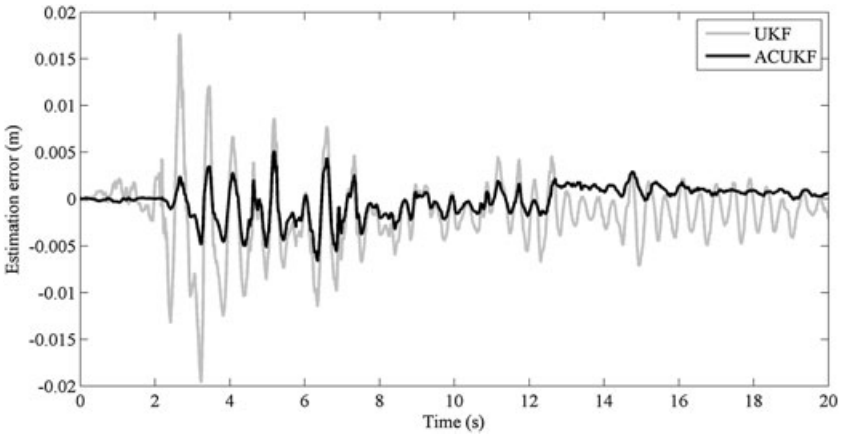

FIGURE 15 Experimental results—Estimation error for the top displacement

The performances of the two estimation algorithms have been evaluated considering as input three measured accelerations: ground, base, and top; base and top displacement estimations have been compared with the measured ones obtained by the laser displacement sensors.

Figure 12 shows the comparison between the measured base displacement and the estimated ones.

Figure 13 shows the comparison between the measured top displacement and the estimated ones.

Both the algorithms are able to estimate with a good approximation the actual displacement of the base and the top of the structure. More in detail, the experimental results highlight that the ACUKF outperform the UKF. This result is clearly shown in Figures 14 and 15 where the time histories of the estimation errors for both the procedures are presented, for the base and the top of the structure, respectively.

Note that the estimation error for the ACUKF is greater at the beginning of the seismic event. This result is strictly related to the choice of initial parameters and the adaptation time of ACUKF as demonstrated by the trend of the estimation error that decreases progressively, demonstrating the convergence of the algorithm.

Figures 16–21 show the estimated parameters.

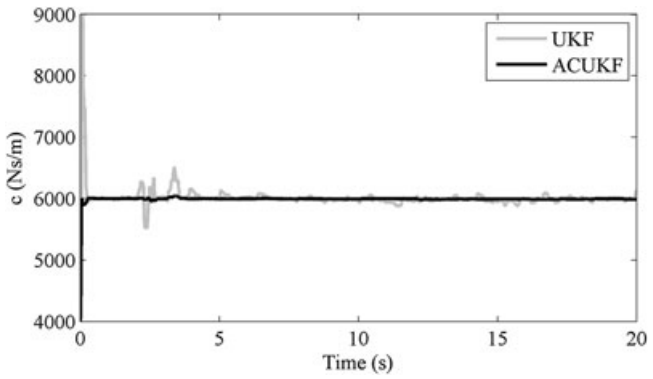

FIGURE 16 Experimental results—Estimation of parameter c

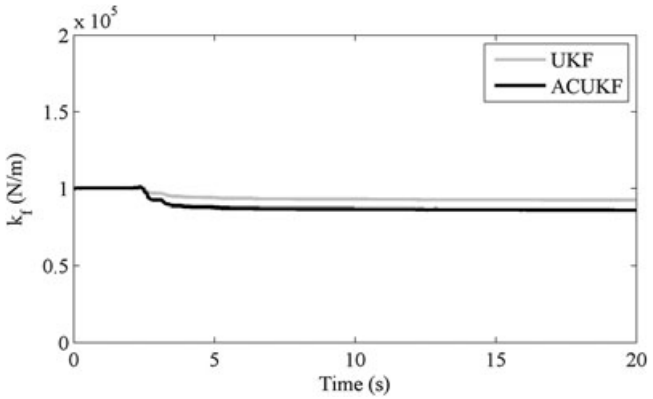

FIGURE 17 Experimental results—Estimation of parameter k_f

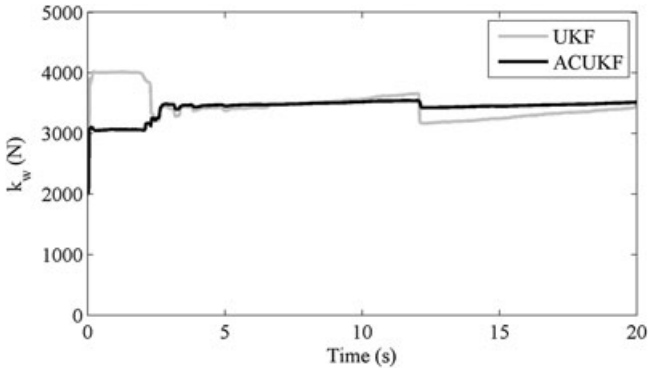

FIGURE 18 Experimental results—Estimation of parameter k_w

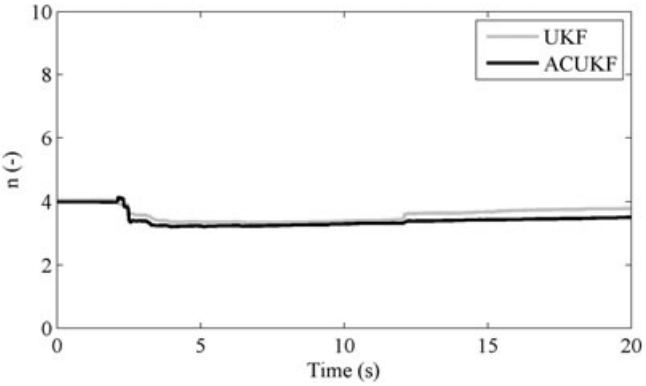

FIGURE 19 Experimental results—Estimation of parameter n

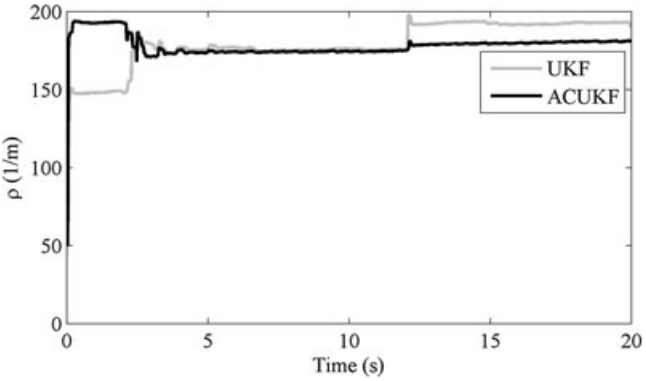

FIGURE 20 Experimental results—Estimation of parameter ρ

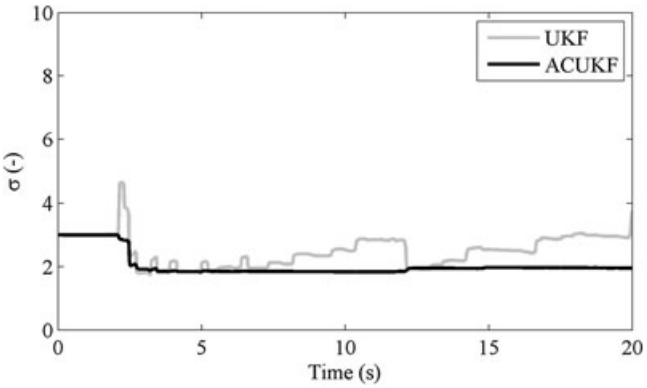

FIGURE 21 Experimental results—Estimation of parameter σ

As observed from Figures 16–21, all the parameters identified with the ACUKF converge to a constant value. Moreover, the estimated NBWM parameters with the UKF and the ACUKF are in accordance with their physical meaning.

5 | CONCLUSIONS

The application of an adaptive constrained unscented Kalman filter (ACUKF) to structural system identification problems is presented in this paper. The performance of the ACUKF is compared with that one of the unscented Kalman filter (UKF).

Numerical results are discussed considering as case study the state estimation and the parameter identification of a nonlinear hysteretic system where the nonlinear behavior follows the NBWM. The ACUKF yields more accurate estimation results than the UKF. The method allows an online determination of the measurement noise covariance matrix, and it takes into account state and parameter boundaries. Numerical results show the ability of the ACUKF to identify a sudden variation of noise level, demonstrating its robustness.

A further comparison between the ACUKF and the UKF is presented based on an experimental activity concerning the displacement estimation of a base-isolated structure starting from acceleration measurements. Experimental results show the convergence of both methods and underline that the ACUKF outperforms the UKF in terms of estimation accuracy and robustness. The ACUKF is computationally efficient, permitting its applicability in adaptive control methodologies where real-time parameter estimation is required.

ACKNOWLEDGEMENTS

The authors deeply thank Giuseppe Iovino and Gennaro Stingo for their technical support.

ORCID

Andrea Calabrese http://orcid.org/0000-0001-7441-9275
Salvatore Strano http://orcid.org/0000-0003-2697-2273

REFERENCES

[1] Y. Lei, Y. Jiang, Z. Xu, *Mech. Syst. Signal Process.* **2012**, *28*, 229.

[2] D. Bernal, *Mech. Syst. Signal Process.* **2013**, *39*, 361.

[3] A. Calabrese, S. Strano, G. Serino, M. Terzo. An extended Kalman filter procedure for damage detection of base-isolated structures (2014) EESMS 2014 - 2014 IEEE workshop on environmental, Energy and Structural Monitoring Systems, Proceedings, art. no. 6923262, pp. 40–45.

[4] J. N. Yang, S. Lin, *ASCE J. Eng. Mech.* **2005**, *131*, 290.

[5] J. N. Yang, S. Lin, H. Huang, L. Zhou, *Struct. Control Health Monit.* **2006**, *13*, 849.

[6] C. M. Pappalardo, D. Guida, *Meccanica* in press, *2016*, https://doi.org/10.1007/s11012-016-0601-1.

[7] T. Sato, M. Chung, *JSCE J. Struct. Eng.* **2006**, *51*, 471.

[8] S. W. Doebling, C. R. Farrar, M. B. Prime, *The Shock and Vibration Digest* **1998**, *30*, 91.

[9] C. M. Pappalardo, D. Guida, *ASME J. Dyn. Syst. Meas. Control.* **2017**, *139*(8), 081010), 1.

[10] L. Humar, A. Bagchi, H. Xu, *Struct. Health Monit.* **2006**, *5*, 215.

[11] E. Manoach, S. Samborski, A. Mitura, J. Warminski, *Int. J. Mech. Sci.* **2012**, *62*(1), 120.

[12] S. Soyoz, M.Q. Feng, E. Safak, Real-time structural health monitoring incorporating soil–structure interaction, Hundredth Anniversary Earthquake Conference, San Francisco, CA **2006**18–22.

[13] T. Furukawa, *Struct. Construct. Eng.* **2009**, *74*, 1113.

[14] E. Ntotsios, C. Karakostas, V. Lekidis, P. Panetsos, I. Nikolaou, C. Papadimitriou, T. Salonikos, *Bull. Earthq. Eng.* **2010**, *7*, 485.

[15] F. Vestroni, *Dyn. Methods for Damage Detect. Struct.* **2010**, *499*, 111.

[16] Z. Xie, J. Feng, *Mech. Syst. Signal Process.* **2012**, *28*, 309.

[17] E. N. Chatzi, A. W. Smyth, *Struct. Control Health Monit.* **2009**, *16*(1), 99.

[18] K. Erazo, E. M. Hernandez, *ASCE-ASME J. Risk Uncertain. Eng. Syst. Part A: Civ. Eng.* **2016**, *2*(3).

[19] Kandepu R, Imsland L, Foss B. Constrained state estimation using the unscented Kalman filter. In: Sixteenth Mediterranean Conference on Control and Automation Congress Centre, Ajaccio, France **2008**.

[20] E. N. Chatzi, A. W. Smyth, S. F. Masri, *Struct. Saf.* **2010**, *32*(5), 326 ISSN 0167-4730.

[21] P. Vachhani, S. Narasimhan, R. Rengaswamy, *J. Process. Control.* **2006**, *16*(10), 1075.

[22] R. Kandepu, B. Foss, L. Imsland, *J. Process Control* **2008**, *18*(7–8), 753.

[23] S. Kolas, B. Foss, T. Schei, *Comput. Chem. Eng.* **2009**, *33*(8), 1386.

[24] R. Mandela, V. Kuppuraj, R. Rengaswmy, S. Narasimhan, *J. Process Control* **2012**, *22*(4), 718.

[25] B. Wu, T. Wang, *Smart. Struct. Syst.* **2014**, *14*(6), 1105.

[26] K. Jiang, E. Cao, L. Wei, *Fuel* **2016**, *165*, 185.

[27] Y. Chae, J. M. Ricles, R. Sause, *Part I: Passive mode. Earthq. Eng. Struct. Synamics* **2013**, *42*, 669.

[28] M. N. Chatzis, E. N. Chatzi, A. W. Smyth, *Earthq. Engng Struct. Dyn.* **2015**, *44*, 523, https://doi.org/10.1002/eqe.2528.

[29] F. Ikhouane, O. Gomis-Bellmunt, *Syst. Control Lett.* **2008**, *57*, 663.

[30] F. Ikhouane, J. Rodellar, *Nonlinear Dyn.* **2005**, *42*, 79.

[31] F. Ikhouane, J. Rodellar, *Nonlinear Dyn.* **2005**, *42*, 63.

[32] Y. Yang, F. Ma, *J. Vib. Control.* **2003**, *9*, 1343.

[33] H. Zhang, G. C. Foliente, Y. Yang, F. Ma, *Earthq. Eng. Struct. Dyn.* **2002**, *3*, 1113.

[34] R. Omrani, R. E. Hudson, E. Taciroglu, *J. Eng. Mech-ASCE* **2013**, *139*(4), 452.

[35] M. Wu, A. W. Smyth, *Struct. Control Health Monit.* **2007**, *14*(7), 971.

[36] S. Mariani, A. Ghisi, *Nonlinear Dyn.* **2007**, *49*(1), 131.

[37] H. Li, Y. Tan, R. Dong and Y. Li, "The unscented Kalman filter for the sandwich system with hysteresis," 2015 34th Chinese Control Conference (CCC), Hangzhou, **2015**, 8293–8297. https://doi.org/10.1109/ChiCC.2015.7260955

[38] S. Eftekhar Azam, A. Ghisi, S. Mariani, A Parallel Implementation of the Sigma-Point Kalman Filter, in *Proceedings of the Tenth International Conference on Computational Structures Technology*, (Eds: B. H. V. Topping, J. M. Adam, F. J. Pallarés, R. Bru, M. L. Romero), Civil-Comp Press, Stirlingshire, UK, Paper 64 **2010** https://doi.org/10.4203/ccp.93.64

[39] Julier, S.J., Uhlrnann, J.K., Durrant-Whyte, H.F.: A new approach for filtering nonlinear systems, in: Proceedings of the American control conference, Seattle, Washington, (**1995**)

[40] Julier S.: The scaled unscented transformation, in: Proceedings of the 2002 American control conference, 6, Anchorage, AK, (**2002**)

[41] A. Calabrese, M. Spizzuoco, G. Serino, G. D. Corte, G. Maddaloni, *Struct. Control Health Monit.* **2015**, *22*(1), 107.

[42] A. Calabrese, G. Serino, S. Strano and M. Terzo, Investigation of the seismic performances of an FRBs Base isolated steel frame through hybrid testing, *Proc. of the World Congress on Engineering WCE 2013*, Vol. III. London, U.K., July 3–5, **2013**,1974–1978.

[43] C. M. Chang, S. Strano, M. Terzo, *Shock. Vib.* **2016**, *2016*, Article ID 3424191, 14, https://doi.org/10.1155/2016/3424191

[44] S. Strano, M. Terzo, *Struct. Control Health Monit.* **2014**, *21*(8), 1193.

How to cite this article: Calabrese A, Strano S, Terzo M. Adaptive constrained unscented Kalman filtering for real-time nonlinear structural system identification. *Struct Control Health Monit*. 2017;e2084. https://doi.org/10.1002/stc.2084